

Numerical and Experimental Studies of Extinguishment of Cup-Burner Flames by $C_6F_{12}O$

Fumiaki Takahashi

Case Western Reserve University, Cleveland, OH 44106, USA

Viswanath R. Katta

Innovative Scientific Solutions, Inc., Dayton, OH 45440, USA

Valeri I. Babushok and Gregory T. Linteris

National Institute of Standards and Technology, Gaithersburg, MD 20899, USA

Proceedings of the Combustion Institute
Volume 38, Issue 3, 2021, Pages 4645-4653

Corresponding Author:

Dr. Fumiaki Takahashi

Department of Mechanical and Aerospace Engineering

Case Western Reserve University

10900 Euclid Avenue

Cleveland, OH 44106, USA

Fax: 1 (216) 368-6838

E-mail: fxt13@case.edu

Abstract

The extinguishment of propane cup-burner flames by a halon-replacement fire-extinguishing agent $C_6F_{12}O$ (Novec 1230) added to coflowing air in normal gravity has been studied computationally and experimentally. The time-dependent, axisymmetric numerical code with a detailed reaction mechanism (up to 141 species and 2206 reactions), molecular diffusive transport, and a radiation model, is used to reveal a unique two-zone flame structure. The peak reactivity spot (i.e., reaction kernel) at the flame base stabilizes a trailing diffusion flame, which is inclined inwardly by a buoyancy-induced entrainment flow. As the volume fraction of the agent in the coflow is increased gradually, the total heat release increases up to three times due to unwanted combustion enhancement by exothermic reactions to form HF and CF_2O in the two-zone trailing flame; whereas at the base, the flame-anchoring reaction kernel weakens (the local heat release rate decreases) and eventually the flame blows off. A numerical experiment, in which the $C_6F_{12}O$ agent decomposition reactions are turned off, indicates that for addition of inert $C_6F_{12}O$, the maximum flame temperature decreases rapidly due to its large molar heat capacity, and the blow-off extinguishment occurs at ≈ 1700 K, a value identical to that for inert gases previously studied, while the reaction kernel is still burning vigorously. The calculated minimum extinguishing concentrations of $C_6F_{12}O$ in a propane flame are 4.2 % (with full chemistry), which coincides with the measured value of 4.17 ± 0.30 %.

Keywords: Aircraft cargo-bay fire suppression; Halon 1301 replacement; Novec 1230; Diffusion flame stabilization; Reaction kernel

1 Introduction

Research for the last two decades to find a replacement for the effective but ozone-destroying fire suppressant Halon 1301 (bromotrifluoromethane, CF_3Br) used in aircraft cargo-bays has made good progress; however, a replacement agent with all of the properties of CF_3Br has not yet been identified. Unlike CF_3Br , some replacement agents failed a mandated Federal Aviation Administration (FAA) Aerosol Can Explosion Test [1, 2] as they caused overpressures due to unwanted combustion enhancement, as has been reported in the literature [3-10]. Based on thermodynamic equilibrium and perfectly stirred-reactor calculations for premixed systems, it was postulated [11-13] that higher overpressures in the FAA aerosol can tests might be due to higher heat release from reaction of the inhibitor itself. Nonetheless, the agents should still reduce the overall reaction rate and inhibit the reaction [14,15] in these stirred-reactor systems since all reactants, intermediates, and products exist simultaneously. In diffusion flames and most fires, however, the flame structure, i.e., the distributions of the temperature, species concentrations, and velocity, play decisive roles in the interactions between the inhibitor and the flame. In turn, such interactions change the flame structure. Therefore, there is an urgent need to study the effects of a potential halon replacement agent on the chemical structure and extinguishment mechanisms of diffusion flames.

In previous papers [16-18], the results of full-chemistry computations of cup-burner flames with CF_3Br , C_2HF_5 (pentafluoroethane, HFC-125), $\text{C}_2\text{HF}_3\text{Cl}_2$ (2,2-dichloro-1,1,1-trifluoroethane, HCFC-123), and $\text{C}_3\text{H}_2\text{F}_3\text{Br}$ (2-bromo-3,3,3-trifluoropropene, 2-BTP) added to the coflowing air were reported. Additional numbers of carbon and fluorine atoms in the halon-replacement-agent molecules, compared to CF_3Br , represent potential energy contributions at a fixed concentration if they burn completely to COF_2 and HF. The combustion enhancement was evident in the computation, particularly with C_2HF_5 or $\text{C}_2\text{HF}_3\text{Cl}_2$ added [18]. For $\text{C}_2\text{HF}_3\text{Cl}_2$ or $\text{C}_3\text{H}_2\text{F}_3\text{Br}$ added, however, the calculation was unable to obtain the converged solution near the extinguishment limit. An attempt was unsuccessful even at low concentrations of one other agent $\text{C}_6\text{F}_{12}\text{O}$ (dodecafluoro-2-methylpentan-3-one, FK-5-1-12, Novec 1230).

$C_6F_{12}O$ is a good agent on a mole basis but (like most other replacements) still quite inferior to CF_3Br on a mass basis. In fact, the mass-basis extinguishing concentration of $C_6F_{12}O$ is comparable to chemically passive gases such as N_2 , CO_2 , CF_4 , and C_4F_{10} , and $C_6F_{12}O$ maybe acts like an inert fire-extinguishing agent. However, the physical and chemical effects of $C_6F_{12}O$ on the diffusion flame structure and extinguishment processes have not yet been fully studied.

This paper extends the prior effort [18] on halon-replacement agents to $C_6F_{12}O$ by overcoming the convergence difficulties in the numerical simulation and by conducting the cup-burner flame extinguishment experiments using propane as the fuel.

2 Experimental Procedures

The standard cup burner [19] consists of a cylindrical glass cup (26 mm i.d., 30 mm o.d.) positioned inside a glass chimney (8.6 cm inner diameter, 45.7 cm height). To provide uniform flow, 6 mm glass beads fill the base of the chimney, and 3 mm glass beads (with a 15.8 mesh/cm screen on top) fill the fuel cup. The gas flow rates are measured by mass flow meters (Hastings HFM-200*), which are calibrated so that their uncertainty is 2 % of indicated flow. The fuel gas used is propane (Airgas CP, 99 %), the air is house compressed air supplied by an oil-free compressor (filtered and dried), and the fire-extinguishing agent is $C_6F_{12}O$ (3M, b.p. 49.2 °C). The flow rate of the liquid agent is metered by a syringe pump (Harvard Scientific, Model 11 Plus) at room temperature. The agent is added to a metered bypass air flow and vaporized completely while flowing through stainless-steel tubing in a temperature-controlled circulation water bath (Fisher Thermo Scientific, Model 2864). Then the agent-air mixture is combined with a main air flow at room temperature at the concentrations below its saturation vapor pressures before entering the cup burner. To determine the minimum extinguishing concentration (MEC), for a fixed mean fuel velocity of 0.307 cm/s, the agent is added (in increments of < 1 % near extinguishment) to the co-

*Certain commercial equipment, instruments, or materials are identified in this paper to adequately specify the procedure. Such identification does not imply recommendation or endorsement by the authors or the funding agencies, nor does it imply that the materials or equipment are necessarily the best available for the intended use.

flowing air at an initial velocity of 10.7 cm/s (which converts the flow rate of 32.8 l/min at 21.1 °C) until extinguishment occurs. The flame-base oscillation occurs just prior to blowoff, as observed previously for CO₂ [32]. The test was repeated 29 times. The MEC value is reported with 95 % confidence interval calculated from $\bar{X} \pm 1.96\sigma/\sqrt{n}$ where \bar{X} is the average value, σ is the standard deviation, and n is the number of samples.

3 Computational Method

The numerical simulation of coflow diffusion flames stabilized on the cup burner is performed using a time-dependent, axisymmetric numerical code (UNICORN) [20,21]. The code solves the axial and radial (z and r) full Navier-Stokes momentum equations, continuity equation, and enthalpy- and species-conservation equations on a staggered-grid system. The buoyancy effect is included in the momentum equation. A clustered mesh system is employed to trace the gradients in flow variables near the flame surface. The thermo-physical properties such as enthalpy, viscosity, thermal conductivity, and binary molecular diffusion of all of the species are calculated from the polynomial curve fits developed for the temperature range 300 K to 5000 K. Mixture viscosity and thermal conductivity are then estimated using the Wilke and Kee expressions [22], respectively. Molecular diffusion is assumed to be of the binary-diffusion type, and the diffusion velocity of a species is calculated using Fick's law and the effective-diffusion coefficient of that species in the mixture. A simple radiation model [23] based on the optically thin media assumption is incorporated into the energy equation. Radiation from CH₄, CO, CO₂, H₂O, HF, and COF₂ was considered in this study. The Plank-mean absorption coefficients are obtained from the literature for the first four species [23] and HF [24]; and calculated for COF₂ [24]). The finite-difference forms of the momentum equations are obtained using an implicit QUICKEST scheme [20], and those of the species and energy equations are obtained using a hybrid scheme of upwind and central differencing.

A comprehensive reaction mechanism for the simulation of propane flames with $C_6F_{12}O$ added to “air” (21 % O_2 in nitrogen) is assembled from the San Diego mechanism 2016 release for C_1 - C_3 hydrocarbons [25] extended to C_4 [26] (58 species and 540 one-way elementary reactions) and a subset (83 species and 1666 reactions) of the NIST HFC mechanism [27,28]. The hydrocarbon combustion mechanism [25,26] is newly employed herein by replacing Ref. [18]. Improvements have been made in the computation mostly on the issues related to the convergence, while maintaining the kinetic data of the HFC mechanism the same. The thermodynamic data for fluorine-containing species [27,28] in the model used previously [13] have been updated with more recent sources [29,30], particularly with relatively large changes for CF_2O [30]. The final chemical kinetics model (141 species and 2206 reactions) is integrated into the UNICORN code.

The boundary conditions are treated in the same way as reported in earlier papers [10,16-18]. The computational domain is bounded by the axis of symmetry, a chimney wall, and the inflow and outflow boundaries. The cup-burner outer diameter is 28 mm and the chimney inner diameter is 95 mm. The wall surface is under the no-slip velocity condition. The wall temperature of the burner (4-mm length and 1-mm thickness tube) is set at 294 K for the inlet portion (3-mm length) and 600 K for the exit portion (1-mm length). Since the cup-burner flame base detaches the burner in a centimeter order, the effect of the wall temperature on the MEC is weak. The value of 600 K is close to the measured values [31,32].

The propane is ignited in the air to form a stable baseline flame. To determine the MEC value, the agent is added incrementally (<1 % near extinguishment) while holding the inflow velocities of the propane fuel and the oxidizer (air+agent) at 0.307 cm/s and 10.7 cm/s, respectively, at 294 K. The MEC value in the cup burner is, in general, nearly constant (plateaued) over a wide oxidizer velocity range (3-18 cm/s) [31]. At each agent increment, the previous solution is used for the initial data consecutively. The present numerical code can capture the flame-base oscillation prior to blowoff extinguishment [32].

Validation of the code with the kinetic model was performed previously through the simulation of opposing-jet diffusion flames. The predicted extinction strain rates for propane-air flames (no agent) were within 7.5 % of the measured values (with an error margin of 9 %) by Zegers et al. [33]. The predicted extinction agent concentrations for CF_3Br and C_2HF_5 are within 4 % of the measured concentrations in weakly stretched flames and within 25 % in highly stretched flames.

4 Results and Discussion

4.1 Extinguishment experiment

The flame base anchors at the burner rim, supports a trailing diffusion flame, and controls the flame attachment, detachment, and oscillation processes [32, 34]. As the $\text{C}_6\text{F}_{12}\text{O}$ is added to the coflowing oxidizing stream, the flame height increases (flares up) substantially and the flame base oscillates inward and outward before blowoff extinguishment. The measured MEC value is 4.17 ± 0.30 % from 29 extinguishment experiments.

4.2 Flame structure

In the computation, as the agent volume fraction in the coflowing oxidizing stream (X_a) approaches the extinguishment limit, the rim-detached flame base location becomes sensitive to small variations of X_a . Figure 1 shows the calculated propane flame structure: (a) an agent-free rim-attached flame, (b) a near-limit detached flame with $\text{C}_6\text{F}_{12}\text{O}$ agent added at $X_a=0.04$, and (c) the same as Fig. 1b with the agent decomposition reactions turned off. The variables include the velocity vectors (\mathbf{v}), isotherms (T), and heat-release rate (\dot{q}). The base of the agent-free flame (Fig. 1a) is anchored at the burner rim. The flame inclines inwardly due to the buoyancy-induced flow. The contours of the heat-release rate show a peak reactivity spot (i.e., the *reaction kernel* [31]). The height from the burner rim (z) at the reaction kernel (the peak \dot{q} point) is $z_k=0.6$ mm, where subscript k is at the reaction kernel. The chain propagation radical species (H, O, and OH) as well as heat diffuse back against the incoming oxygen-rich flow at the flame base (edge), thus promoting vigorous reactions at the reaction kernel. For the burner rim-attached flame

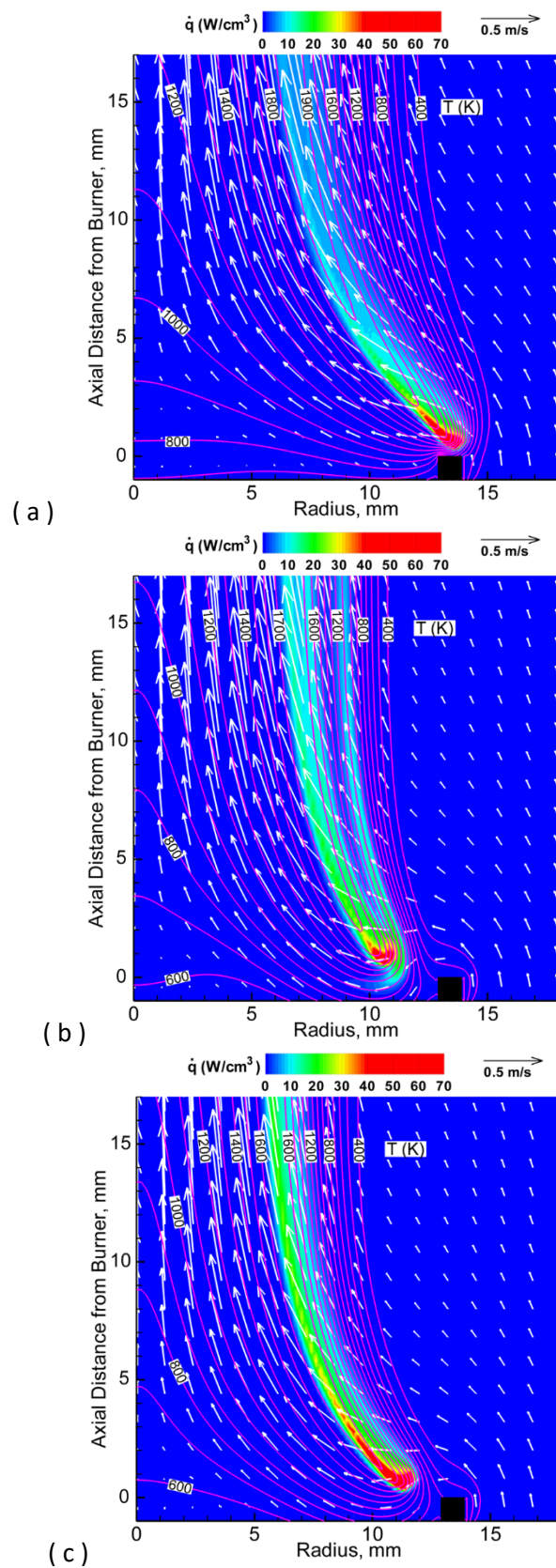


Fig. 1 Calculated propane flame structure: (a) an agent-free flame, (b) a near-limit flame with added $C_6F_{12}O$ at $X_a=0.04$ by full-chemistry, and (c) a near-limit flame with $C_6F_{12}O$ agent added at $X_a=0.04$ with the agent decomposition reactions turned off.

(Fig. 1a), the temperature gradient near the reaction kernel may be affected by the wall temperature. The values of the variables at the reaction kernel are $\dot{q}_k=141.9 \text{ W/cm}^3$, $|\mathbf{v}_k|=0.215 \text{ m/s}$, and $T_k=1478 \text{ K}$, where $|\mathbf{v}|$ is the magnitude of the velocity vector \mathbf{v} .

For the near-limit flame (Fig. 1b), the flame base is pushed inward by the nearly horizontal (and even slightly downward) entrainment flow. At the MEC condition (not shown), the cup-burner flame base lifts off a centimeter order, and the fuel-velocity (0.307 cm/s) effect on the MEC is weak. The heat-release rate contours show the two-zone flame structure downstream as reported previously [18] for C_2HF_5 and $\text{C}_2\text{HF}_3\text{Cl}_2$. The values of the variables at the reaction kernel are $\dot{q}_k=66.8 \text{ W/cm}^3$, $|\mathbf{v}_k|=0.207 \text{ m/s}$, and $T_k=1510 \text{ K}$. The heat release rate is reduced substantially.

For the near-limit flames with the agent decomposition reactions turned off (Fig. 1c), the flame base is pushed inward as well but with a single trailing flame zone. The values of the variables at the reaction kernel are $\dot{q}_k=122.4 \text{ W/cm}^3$, $|\mathbf{v}_k|=0.158 \text{ m/s}$, and $T_k=1411 \text{ K}$. The heat release rate is not reduced as much as the full chemistry case (Fig. 1b).

The heat-release rate contour shape (Fig. 1b) resembles the tribrachial (or triple) flame structure—the stoichiometric diffusion flame with the fuel rich and lean premixed flame branches—at a glance. However, the outer reaction zone and the small wing below the reaction kernel are formed by the reactions of agent itself along a temperature contour of $\approx 1100 \text{ K}$. It is evidences by the results for no agent reactions (Fig. 1c), in which the outer zone disappears. The present full-chemistry computation reveals the complex flame structure as described below.

Figure 2 shows the radial variations of the temperature and the heat-release rate, calculated with full chemistry, across the reaction kernel and the trailing flame with $\text{C}_6\text{F}_{12}\text{O}$ added at $X_a=0.04$ at $z=0.8 \text{ mm}$ (z_k) and 5.8 mm ($z_k+5 \text{ mm}$) (see Fig. 1b). At $z=0.8 \text{ mm}$, the heat-release rate peaks at the reaction kernel. At $z=5.8 \text{ mm}$, the flame is characterized by the two-zone structure (inner and outer) as is evident from two main heat-release rate peaks. The inner zone ($7.5 \text{ mm} < r < 9 \text{ mm}$) with two small humps is formed by the

hydrocarbon-O₂ combustion near the temperature peak (1754 K) and fluorine reactions. The outer zone (9 mm < r < 10.5 mm) is formed by exothermic reactions of agent fragments around 1100 K.

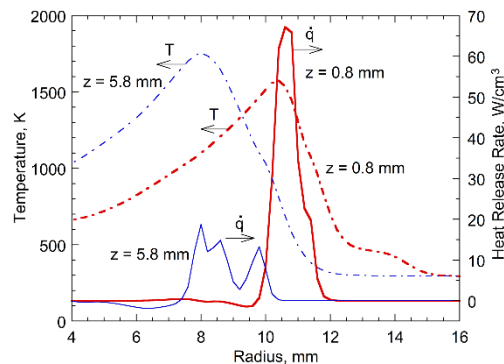


Fig. 2 Radial variations of the temperature and the heat-release rate with added C₆F₁₂O at $X_a=0.04$ by full chemistry across the reaction kernel ($z_k = 0.8$ mm) and the trailing flame ($z_k + 5$ mm = 5.8 mm).

Figure 3 shows the radial variations of the species volume fractions (X_i), calculated with full chemistry, across the reaction kernel and the trailing flame with C₆F₁₂O (added at $X_a=0.04$) at (a) $z=0.8$ mm (z_k) and (b) 5.8 mm (z_k+5 mm). At the height across the reaction kernel (Fig. 3a), some species such as C₃H₈, O₂, and fluorine-containing species are observed on both sides because they diffuse or flow through the quenched space between the flame base and the burner rim. At the height 5 mm above the reaction kernel (Fig. 3b), oxygen penetrates through the outer zone and the C₆F₁₂O agent decomposes to fluorine-containing species by going through the outer reaction zone. A pool of chain carrier radicals (H, O, and OH) as well as F atom are formed in the middle of the two zones at relatively high concentrations ($X_a \approx 10^{-3}$), thus contributing to both reaction zones. The F atom peak with C₆F₁₂O addition is significant compared to C₂HF₅ studied previously [18]. The C₃H₈ fuel diffuses from the fuel side, decomposes to fragments (CH₄, C₂H₄, and C₂H₂), and reacts with the chain carrier radicals in the inner zone. The H₂ and H₂O molecules formed in the inner hydrocarbon-O₂ reaction zone are attacked by the F atom to form HF through the exothermic reactions (which contribute to the second hump in the inner zone). In the outer

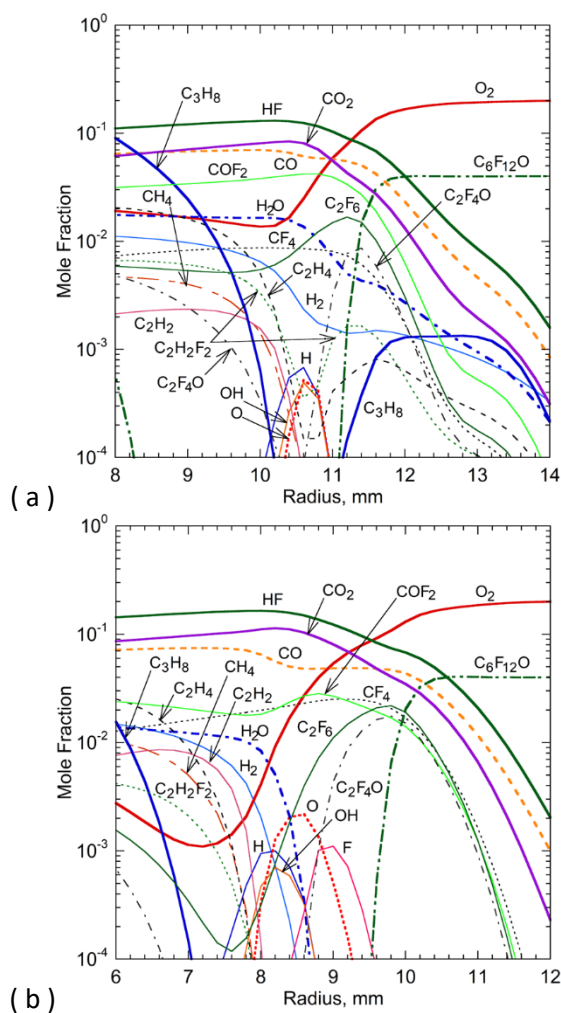


Fig. 3 Radial variations of the species volume fractions with added $C_6F_{12}O$ at $X_a=0.04$ by full-chemistry: (a) across the reaction kernel, $z_k = 0.8$ mm; and (b) the trailing flame, $z_k + 5$ mm = 5.8 mm.

zone, the agent ($C_6F_{12}O$) from the air side decomposes and diminishes, thus resulting in many fragmented fluorinated species (C_2F_4O , C_2F_6 , CF_4 , CF_2O , and others [not shown]), which react with the radicals or penetrate through the inner reaction zone. The exothermic reactions of the fluorinated species form the secondary heat-release rate peak (outer zone) around 1100 K in the high-temperature zone created by the inner zone. Thus the outer zone may not have been self-sustained without interactions with the inner zone. The final products (CO_2 , HF , and CF_2O) and intermediates (CO and CF_4 .) diffuse over a wide range at relatively high concentrations.

4.2 Flame characteristics

Figure 4 shows the effects of the agent volume fraction (X_a) on the calculated coordinates of the reaction kernel (peak heat-release-rate spot), in terms of the axial distance from the burner exit (z_k) and the radius from the axis (r_k), for the full chemistry and without agent decomposition reactions. In both cases, for $0 < X_a < 0.025$, z_k increases slightly (0.6 mm to 0.8-1.0 mm), while r_k decreased gradually (13.4 mm to 12.8 mm), and thus reaction kernel just above the burner rim (see Fig. 1a) moves inside. For $0.025 < X_a < 0.04$, z_k decreases back to ≈ 0.7 mm, while r_k decreased more rapidly to ≈ 11 mm (see Figs. 1b and 1c). As r_k decreases, the agent-laden air flows onto the fuel side and the fuel diffuses onto the oxidizer side over the standoff distance between the flame base and the burner rim, and thus more premixing occurs. As the extinguishment limit is approached ($X_a > 0.04$), the flame base oscillation occurs and thus both z_k and r_k fluctuate until finally, blowoff-type extinguishment occurs.

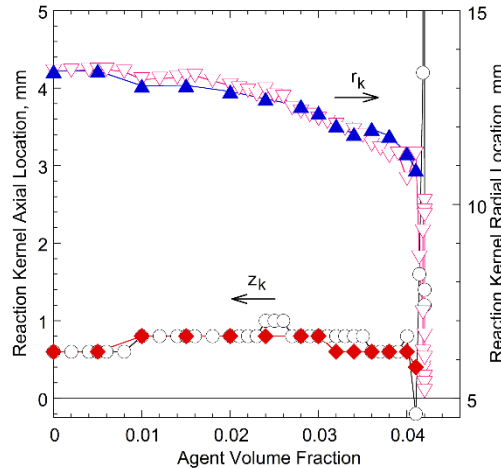


Fig. 4 Calculated axial (z_k) and radial (r_k) positions of the reaction kernel from the burner exit on the axis. Open: full chemistry. Closed: without agent decomposition reactions.

The calculated MEC of $C_6F_{12}O$ for the full-chemistry calculation is 4.2 %, which coincides with the measured MEC value of 4.17 ± 0.30 %. The calculated MEC of $C_6F_{12}O$ without the agent decomposition is 4.3 %. Although the MEC values are close each other with and without the agent decomposition, it does not necessarily mean that the extinguishment occurs solely by the physical effect.

The incoming flow velocity around the flame base is important to diffusion flame stability as it represents the reciprocal of the residence time through the reaction kernel. Figure 5 shows the effects of X_a on the calculated total ($|\mathbf{v}_k|$), axial (U_k), and radial velocity (V_k) at the reaction kernel for the full-chemistry calculation and without the agent decomposition. Variations in velocities correlate with the behavior of z_k and r_k (Fig. 4). For the full-chemistry, for $0 < X_a < 0.025$, U_k decreases to near zero value, while V_k 's absolute value and $|\mathbf{v}_k|$ increase. For $0.025 < X_a < 0.04$, as the reaction kernel moves inside the burner rim, U_k becomes negative, while V_k 's absolute value and $|\mathbf{v}_k|$ decrease. As X_a approaches the MEC, U_k fluctuates with the flame-base oscillation, while V_k decreases to near zero value, and eventually, U_k and thus $|\mathbf{v}_k|$ increases beyond the upper limit of the plot at the blowoff extinguishment. In the case of no agent decomposition, V_k 's absolute value and $|\mathbf{v}_k|$ are much smaller and the variations are monotonic compared to the full-chemistry case.

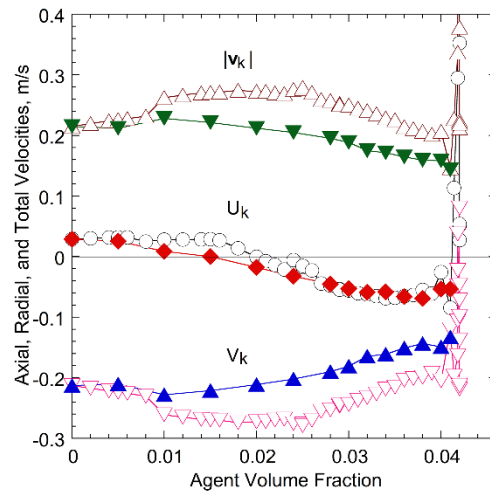


Fig. 5 Calculated total ($|\mathbf{v}_k|$), axial (U_k), and radial velocity (V_k) at the reaction kernel. Open: full chemistry. Closed: without the agent decomposition.

Figure 6 shows the calculated variables at the reaction kernel: the temperature (T_k), heat-release rate (\dot{q}_k), and ratio of the square-root of the heat-release rate and the total velocity ($\sqrt{\dot{q}_k}/|\mathbf{v}_k|$) for the full chemistry and without agent decomposition reactions. For the former case, as X_a is increased for $0 < X_a$

< 0.04 , the reaction kernel temperature maintains at ≈ 1500 K, while the heat-release rate decreases to a half value (≈ 140 to ≈ 70 W/m³). The quantity $\sqrt{\dot{q}_k}/|\mathbf{v}_k|$ relates to a ratio of the residence time and the reaction time, i.e., a local Damkhöler number, at the reaction kernel. As the laminar flame speed of premixed flames is proportional to the square-root of the reaction rate, the new variable is used instead of $\dot{q}_k/|\mathbf{v}_k|$ [34]. The quantity $\sqrt{\dot{q}_k}/|\mathbf{v}_k|$ decreases gradually to a nearly constant level of ≈ 0.4 (Js/cm⁵)^{1/2}, which corresponds to $\dot{q}_k/|\mathbf{v}_k| \approx 3.2$ J/cm⁴ and is consistent with other agents (C₂HF₅, C₂HF₃Cl₂, and C₃H₂F₃Br) [18] and the chemically passive agents [35, 36]. This result suggests that the reaction kernel shifted downstream (smaller r_k) to seek a location where a subtle balance between the residence time and the reaction time can be achieved. As the flame base lifted higher and oscillates in the higher velocity field, it becomes difficult to obtain the balance, thus leading eventually to blowoff.

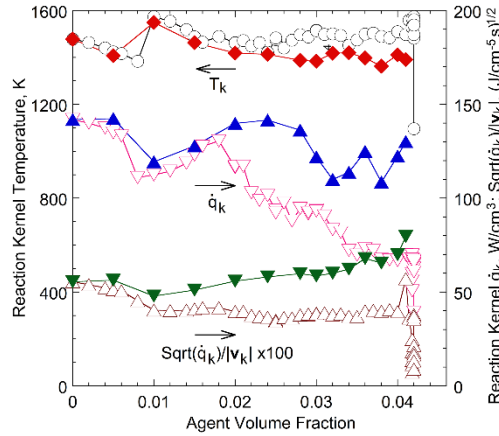


Fig. 6 Calculated temperature, heat-release rate, and a ratio of the heat-release rate and the total velocity at the reaction kernel. Open: full chemistry. Closed: without the agent decomposition.

Figure 7 shows the maximum temperature (T_{\max}) in the trailing diffusion flame, the total heat release, integrated over the entire flame (\dot{q}_{total}) and over the flame base region ($\dot{q}_{<z_k+3 \text{ mm}}$), for the full chemistry and without agent decomposition reactions. Thus, both the heat-release rate per unit volume along the flame zone and the flame height affect the \dot{q}_{total} . For the full-chemistry calculation, unlike the other chemically active agents previously studied [18], for which T_{\max} remains constant at ≈ 1800 K (C₂HF₅

and $C_2HF_3Cl_2$) or mildly increases (CF_3Br or $C_3H_2F_3Br$), T_{max} with added $C_6F_{12}O$ decreases linearly. On the other hand, as X_a is increased 0 to 0.04, \dot{q}_{total} (over the entire flame) increases (i.e., combustion enhancement) about three times (75 to 225 W) with added $C_6F_{12}O$. By contrast, for $0 < X_a < 0.025$, $\dot{q}_{<z_k+3 \text{ mm}}$ is nearly constant. For $0.025 < X_a < 0.04$, during which the reaction kernel detaches the burner rim, $\dot{q}_{<z_k+3 \text{ mm}}$ increases rapidly to form a peculiar peak around $X_a < 0.034$. However, the contribution of the flame base region to the total heat release is still relatively small. Thus, the combustion enhancement occurred much more strongly in the trailing flame. Therefore, the trailing *diffusion* flame burns more with the additional heat release to form HF and CF_2O in the two-zone flame structure, while the reaction kernel with a *premixed* flame nature weakens and blows off eventually. For the calculation without the agent decomposition, T_{max} also decreases linearly but slightly more rapidly with X_a , and the

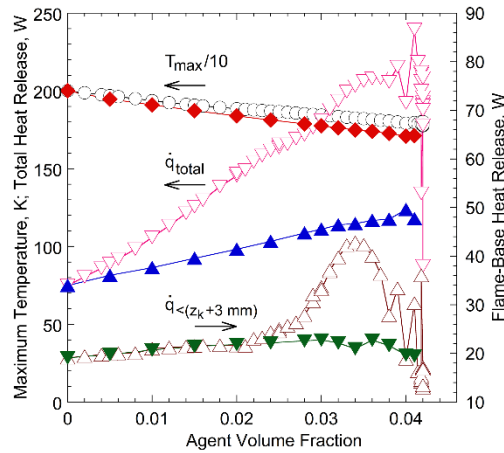


Fig. 7 Calculated maximum temperature (T_{max}) in the trailing diffusion flame, the total heat-release rate (\dot{q}_{total}), integrated over the entire flame and over the flame base region ($\dot{q}_{<z_k+3 \text{ mm}}$). Open: full-chemistry. Closed: without the agent decomposition.

extinguishment occur at $T_{max} \approx 1700$ K, which is the critical condition as same as the chemically passive agents (CO_2 , N_2 , Ar, and He) previously studied [35,36]. For $0 < X_a < 0.04$, \dot{q}_{total} increases linearly about 35 % (75 to 124 W) with added $C_6F_{12}O$ and $\dot{q}_{<z_k+3 \text{ mm}}$ stayed nearly constant without the peak observed for the full chemistry.

5 Conclusions

The interactions of the fire-extinguishing agent $C_6F_{12}O$ and the cup-burner diffusion flame structure, leading to extinguishment, are studied numerically and experimentally. The $C_6F_{12}O$ added to the coflowing air weakens the flame-holding reaction kernel in the flame base. The reaction kernel detaches from the burner rim and moves to a location where a ratio of the residence time and the reaction time (i.e., Damkhöler number) is maintained. As the flame base moves away and oscillates in the higher velocity field, the subtle balance is lost and the blowoff extinguishment occurs. The calculated minimum extinguishing concentrations of $C_6F_{12}O$ in a propane flame (with full chemistry) is 4.2 %, which coincides with the measured value of 4.17 ± 0.30 %.

On the other hand, $C_6F_{12}O$ enhances combustion in the trailing diffusion flame downstream. The two-zone flame structure consists of the inner flame zone of the propane combustion and the outer zone of $C_6F_{12}O$ reactions along the 1100 K contours. The calculated total heat-release triples at the MEC with $C_6F_{12}O$ added, which is much larger than C_2HF_5 and $C_2HF_3Cl_2$ previously studied. In the experiment, the flame flares up with added $C_6F_{12}O$, resulting in substantially larger flame height. $C_6F_{12}O$ is obviously chemically active due to the large numbers of carbon and fluorine atoms in the molecule. In the case of no $C_6F_{12}O$ decomposition reactions, the maximum flame temperature reduces linearly and the extinguishment occurs at ≈ 1700 K, which is identical to the inert gases previously studied.

This work demonstrates that the unwanted combustion enhancement occurs due to inherent diffusion-flame (fire) structure, where the agent in the air reacts exothermically before reaching the main flame zone to inhibit combustion. Therefore, it is imperative to scrutinize compounds to avoid combustion enhancement, among other properties, in search for more effective halon replacement agents.

Acknowledgments

The work at Innovative Scientific Solutions and Case Western Reserve University was supported in part by the Air Force Small Business Initiative Research program (Contract Number: FA9101-17-P-0092) and the National Science Foundation (Grant Number: 1842067). Assistance in conducting the experiment by Wilson Fisher and Samuel Faulk is acknowledged.

References

1. J.W. Reinhardt, Behavior of Bromotrifluoropropene and Pentafluoroethane When Subjected to a Simulated Aerosol Can Explosion, DOT/FAA/AR-TN04/4, 2004.
2. J.W. Reinhardt, Minimum Performance Standard for Aircraft Cargo Compartment Halon Replacement Fire Suppression Systems (2nd Update), DOT/FAA/AR-TN05/20, 2005.
3. I.O. Moen, S.A., Ward, P.A. Thibault, J.H. Lee, R. Knystautas, T. Dean, C.K. Westbrook, The influence of diluents and inhibitors on detonations, Proc. Combust. Inst. 20 (1984) 1717-1725.
4. C.K. Westbrook, Numerical Modeling of Flame Inhibition by CF_3Br , Combust. Sci. Technol. 34 (1-6) (1983) 201-225.
5. G.W. Gmurczyk, W.L. Grosshandler, Suppression of high-speed C_2H_4 /air flames with C_1 -halocarbons, Proc. Combust. Inst. 25 (1994) 1497-1503.
6. Y.N. Shebeko, V.V. Azatyan, I.A. Bolodian, V.Y. Navzenya, S.N. Kopyov, D.Y. Shebeko, E.D. Zamishevski, The influence of fluorinated hydrocarbons on the combustion of gaseous mixtures in a closed vessel, Combust. Flame 121 (3) (2000) 542-547.
7. E. Ikeda and J.C. Mackie, An experimental and modelling study of ignition delays in shock-heated ethane-oxygen-argon mixtures inhibited by 2H-heptafluoropropane, Int. J. Research in Phys. Chem. & Chem. Phys. 215 (8) (2001) 997-1009.
8. J.R. Mawhinney, B.Z. Dlugogorski, A.K. Kim, A Closer Look at the Fire Extinguishing Properties of Water Mist, in: Fire Safety Science—Proceedings of the Fourth International Symposium, International Association for Fire Safety Science, 1994.
9. A. Hamins, K. McGrattan, G.P. Forney, Unwanted Accelerated Burning After Suppressant Delivery, NIST SP-1004, National Institute of Standards and Technology, Gaithersburg, MD, 2003.
10. V.R. Katta, F. Takahashi, G.T. Linteris, Fire-suppression characteristics of CF_3H in a cup burner, Combust. Flame 144 (4) (2006) 645-661.

11. G.T. Linteris, F. Takahashi, V.R. Katta, H. Chelliah, Thermodynamic analysis of suppressant-enhanced overpressure in the FAA Aerosol Can Simulator, in *Fire Safety Science—Proceedings of the Tenth International Symposium*, International Association for Fire Safety Science, 2011.
12. G.T. Linteris, D.R. Burgess, V.R. Katta, F. Takahashi, H.K. Chelliah, O. Meier, Stirred-reactor calculations to understand unwanted combustion enhancement by potential halon replacements, *Combust. Flame* 159 (3) (2012) 1016-1025.
13. G.T. Linteris, V.I. Babushok, P.B. Sunderland, F. Takahashi, V.R. Katta, O. Meier, Unwanted combustion enhancement by $C_6F_{12}O$ fire suppressant, *Proc. Combust. Inst.* 34 (2012) 2683-2690.
14. G.T. Linteris, L. Truett, Inhibition of premixed methane-air flames by fluoromethanes, *Combust. Flame* 105 (1-2) (1996) 15-27.
15. G.T. Linteris, D.R. Burgess, V.I. Babushok, M. Zachariah, W. Tsang, P. Westmoreland, Inhibition of premixed methane-air flames by fluoroethanes and fluoropropanes, *Combust. Flame* 113 (1-2) (1998) 164-180.
16. F. Takahashi, G.T. Linteris, V.R., Katta, O.C. Meier, Cup-burner flame structure and extinguishment by C_2HF_5 in microgravity, *Proc. Combust. Inst.* 34 (2012) 2707-2717.
17. F. Takahashi, V.R., Katta, G.T. Linteris, Combustion inhibition and enhancement of cup-burner flames by CF_3Br , C_2HF_5 , $C_2HF_3Cl_2$, and $C_3H_2F_3Br$, *Proc. Combust. Inst.* 35 (2015) 2741–2748.
18. F. Takahashi, V.R., Katta, G.T. Linteris, V.I. Babushok, A computational study of extinguishment and enhancement of propane cup-burner flames by halon and alternative agents, *Fire Safety J.* 91 (2017) 688-694.
19. Anon, *Standard on Clean Agent Fire Extinguishing Systems*, National Fire Protection Association, NFPA 2001, Quincy, MA (2000).
20. V.R., Katta, L.P. Goss, W.M. Roquemore, Numerical investigations of transitional H_2/N_2 jet diffusion flames, *AIAA J.* 32 (1) (1994) 84.

21. W.M. Roquemore, V.R., Katta, Role of flow visualization in the development of UNICORN, J. Visualization 2 (3, 4) (2000) 257-272.
22. J.O. Hirschfelder, C.F. Curtis, R.B. Bird, The Molecular Theory of Gases and Liquids, Wiley, New York, 1954.
23. R.S. Barlow, A.N. Karpetis, J.H. Frank, J.-Y. Chen, [Scalar profiles and NO formation in laminar opposed-flow partially premixed methane/air flames](#), Combust. Flame 127 (3) (2001) 2102-2118.
24. S.P. Fuss, A. Hamins, Determination of Plank mean absorption coefficients for HBr, HCl, and HF, J. Heat Transfer – Transaction of the ASME 124 (1) (2002) 26-29.
25. "Chemical-Kinetic Mechanisms for Combustion Applications", San Diego Mechanism web page, Mechanical and Aerospace Engineering (Combustion Research), University of California at San Diego (<http://combustion.ucsd.edu>).
26. J.C. Prince, C. Trevino, F.A. Williams, A reduced reaction mechanism for the combustion of n-butane, Combust. Flame 175 (1) (2017) 27-33.
27. D. Burgess, M.R. Zachariah, W. Tsang, P.R. Westmoreland, Thermochemical and chemical kinetic data for fluorinated hydrocarbons, Prog. Energy Combust. Sci. 21 (6) (1995) 453-529.
28. D. Burgess, M.R. Zachariah, W. Tsang, P.R. Westmoreland, Thermochemical and chemical kinetic data for fluorinated hydrocarbons, NIST Technical Note 1412, National Institute of Standards and Technology, Gaithersburg, MD, 1995.
29. A. Ganyecz, M. Kallay, J. Csontos, High accuracy quantum chemical and thermochemical network data for the heats of formation of fluorinated and chlorinated methanes and ethanes. J. Phys. Chem. A, 122 (28) (2018) 5993-6006.
30. E. Goos, A. Burcat, B. Ruscic, Extended Third Millennium Thermodynamic Database for Combustion and Air-Pollution Use with updates from Active Thermochemical Tables [Online], Aerospace Engineering, Technion-IIT Haifa Israel, 2012. Available:

<ftp://ftp.technion.ac.il/pub/supported/aetdd/thermodynamics/BURCAT.THR> [Accessed August 2012].

31. F. Takahashi, G.T. Linteris, V.R., Katta, Extinguishment mechanisms of coflow diffusion flames in a cup-burner apparatus, *Proc. Combust. Inst.* 31 (2007) 2721-2729.
32. F. Takahashi, G.T. Linteris, V.R., Katta, Vortex-coupled oscillations of edge diffusion flames in coflowing air with dilution, *Proc. Combust. Inst.* 31 (2007) 1575-1582.
33. E. J. P. Zegers, B.A. Williams, E.M. Fisher, J.W. Fleming, R.S. Sheinson, Suppression of nonpremixed flames by fluorinated ethanes and propanes, *Combustion and Flame* 121 (3) (2000) 471-487.
34. F. Takahashi, V.R. Katta, A reaction kernel hypothesis for the stability limit of methane jet diffusion flames, *Proc. Combust. Inst.* 28 (2000) 2071-2078.
35. F. Takahashi, G.T. Linteris, V.R., Katta, Extinguishment of methane diffusion flames by carbon dioxide in coflow air and oxygen-enriched microgravity environments, *Combust. Flame* 155 (1-2) (2008) 37-53.
36. F. Takahashi, G.T. Linteris, V.R., Katta, Extinguishment of methane diffusion flames by inert gases in coflow air and oxygen-enriched microgravity environments, *Proc. Combust. Inst.* 33 (2011) 2531-2538.

Figure Captions

- Fig. 1 Calculated propane flame structure: (a) an agent-free flame, (b) a near-limit flame with added $C_6F_{12}O$ at $X_a=0.04$ by full-chemistry, and (c) a near-limit flame with $C_6F_{12}O$ agent added at $X_a=0.04$ with the agent decomposition reactions turned off.
- Fig. 2 Radial variations of the temperature and the heat-release rate with added $C_6F_{12}O$ at $X_a=0.04$ by full chemistry across the reaction kernel ($z_k = 0.8$ mm) and the trailing flame ($z_k + 5$ mm = 5.8 mm).
- Fig. 3 Radial variations of the species volume fractions with added $C_6F_{12}O$ at $X_a=0.04$ by full-chemistry: (a) across the reaction kernel, $z_k = 0.8$ mm; and (b) the trailing flame, $z_k + 5$ mm = 5.8 mm.
- Fig. 4 Calculated axial (z_k) and radial (r_k) positions of the reaction kernel from the burner exit on the axis. Open: full chemistry. Closed: without agent decomposition reactions.
- Fig. 5 Calculated total ($|v_k|$), axial (U_k), and radial velocity (V_k) at the reaction kernel. Open: full chemistry. Closed: without the agent decomposition.
- Fig. 6 Calculated temperature, heat-release rate, and a ratio of the heat-release rate and the total velocity at the reaction kernel. Open: full chemistry. Closed: without the agent decomposition.
- Fig. 7 Calculated maximum temperature (T_{max}) in the trailing diffusion flame, the total heat-release rate (\dot{q}_{total}), integrated over the entire flame and over the flame base region ($\dot{q}_{<z_k+3}$ mm). Open: full-chemistry. Closed: without the agent decomposition.